

Wavelength selection for the far-infrared p-Ge laser using etched silicon lamellar gratings

T.W. Du Bosq^a, R.E. Peale^{a,*}, E.W. Nelson^a, A.V. Muravjov^{a,1}, D.A. Walters^a,
G. Subramanian^b, K.B. Sundaram^b, C.J. Fredrickson^c

^aDepartment of Physics, University of Central Florida, Orlando, FL 32816, USA

^bDepartment of Electrical and Computer Engineering, University of Central Florida, Orlando, FL 32816, USA

^cZaubertek, Inc. 12565 Research Parkway Suite 300, Orlando, FL 32826, USA

Received 26 August 2003; accepted 17 February 2004

Abstract

A lamellar mirror made from Si wafer by anisotropic chemical etching and coated with gold has been demonstrated as an intracavity wavelength selector for the far-infrared p-Ge laser. The etching process produces rectangular grooves with precisely predetermined depth and 100 nm surface smoothness. This lamellar-grating structure defines the resonant laser wavelength within the broad tuning range of the p-Ge laser. Single wavelength laser operation with this mirror has been demonstrated on the third-order resonance with an active cavity finesse of at least 0.09.

© 2004 Elsevier Ltd. All rights reserved.

Keywords: Terahertz; Germanium; Laser

1. Introduction

With its high peak power (1 W) and broad tuning range (1.5–4.2 THz, 70–200 μm), a p-Ge laser [1] with practical means of selecting a narrow emission line would have value in chemical spectroscopy and sensing. Recent advances in quantum cascade laser (QCL) technology provides laser emission at any wavelength within the same THz range spanned by the p-Ge laser [2,3]. However, each new wavelength requires development and molecular beam epitaxy of a new QCL structure. This paper presents a relatively simple method of selecting wavelength using the p-Ge laser with selective lamellar mirror.

Because of the anomalously wide p-Ge laser gain bandwidth, the spectrum of the laser emission is approximately 20 cm^{-1} wide unless special selectors are used. For the usual cavity lengths (> 10 cm) determined by optical length of the active crystal, this 20 cm^{-1} band contains several hundred

longitudinal modes. Intra-cavity wavelength selection based on lamellar gratings [4] have been reported [5,6], where the active cavity finesse can exceed unity, which results in single longitudinal mode emission [7]. Piezo-control of the selector has allowed fine tuning between nearby longitudinal modes [8]. A variable-length cavity was demonstrated, which in principle allows continuous tuning without mode hops [9].

Selector design has been constrained by the cryogenic environment, high operating voltages, and high index of refraction of germanium. In the tunable lamellar-gratings used to date, a silicon spacer has supported aluminum stripes and isolated the high-voltage laser-excitation pulse from the metal tuner parts [5–8]. A disadvantage of this design is the appearance of unwanted wavelength-selective resonances introduced by the silicon spacer itself [8,10]. The pattern of evaporated stripes is difficult to experimentally optimize for highest selector Q. Also, a piston [5–8] that assures parallel changes in the air gap of the tuner tends to stick at the cryogenic p-Ge laser operating temperatures. When this piston is piezo-controlled, only small displacements can be achieved even with high control voltages, resulting in a limited tuning range [8]. This problem is compounded by the four-fold reduction of piezo action upon cooling to 4 K.

* Corresponding author. Tel.: +1-407-823-5208; fax: +1-407-823-5112.

E-mail address: rep@physics.ucf.edu (R.E. Peale).

¹ On leave from Institute for Physics of Microstructures, RAS, Nizhny Novgorod, Russia.

Clearly, new selector concepts are required for the p-Ge laser. A promising approach toward developing new selector designs is silicon process technology. Recently, we demonstrated a fixed wavelength selector based on a simple silicon intracavity etalon [11,12]. In this paper, we explore a new type of fixed wavelength selector made by etching a lamellar structure into silicon, which is then coated with gold and used as a back mirror.

2. Experimental details

Silicon micromachining takes advantage of anisotropic alkaline-type etchants. Tetramethyl ammonium hydroxide (TMAH) is an effective wet etchant, which produces smooth mirror-like etched surfaces. The etch rates vary from 0.5 to 1.4 $\mu\text{m}/\text{min}$ and 0.1–0.2 $\mu\text{m}/\text{min}$ at 80°C for [1 0 0] and [1 1 0] silicon, respectively. Orientation-dependent etching for [1 1 0]-oriented silicon through a patterned SiO_2 mask creates nearly straight-walled grooves with [1 1 1]-side planes. Deep vertical cavities up to 150 μm can be fabricated with a depth control of 1 μm .

Mask patterns produced using AutoCAD were transferred as chrome onto a 63.5 mm \times 63.5 mm \times 1.52 mm soda lime glass plate with a critical dimension tolerance $\pm 10 \mu\text{m}$ by Adtek Photomask. Silicon wafers ([1 1 0]-oriented, 50 mm diameter, single side polished) were oxidized to produce an etch mask layer. Negative photoresist was spun on and then baked at 150°C for 1 min. The mask pattern was applied using a mask aligner and 10 s exposure. The wafer was then baked at 100°C for 1 min and developed, after which the wafer was baked at 150°C for 3 min. The oxide in the masked areas was stripped using buffered oxide etch (BOE). Acetone and methanol removed the remaining photoresist and the exposed silicon was etched for 2 h with 20 parts TMAH, 70 parts deionized water, and 10 parts isopropyl alcohol at 90°C. Isopropyl alcohol was added at regular intervals to insure smooth surfaces. The wafer was removed from the etching bath and immersed in BOE to strip the remaining oxide.

A table-top sputtering system evacuated by a mechanical pump without trap deposited 150 nm of AuPd onto the etched mirror. The samples were removed and transferred to an evaporator for a 450 nm coating of Au to give it high far-IR reflectivity. The depth of the trenches was determined with an optical microscope. Taking the difference between the focus of the top of the selector and the bottom of the trench, the depth was determined with an uncertainty of 5 μm . Width of features in the plane was determined using a micrometer controlled translation stage and the optical microscope, which was equipped with a cross-hair eyepiece.

An atomic force microscope (AFM; Veeco Metrology Nanoscope IIIA) characterized roughness and surface features of one finished mirror. To image the bottom surface of the trenches, the front corners of the cantilever chip (TAP300, Nanodevices) were mechanically removed by

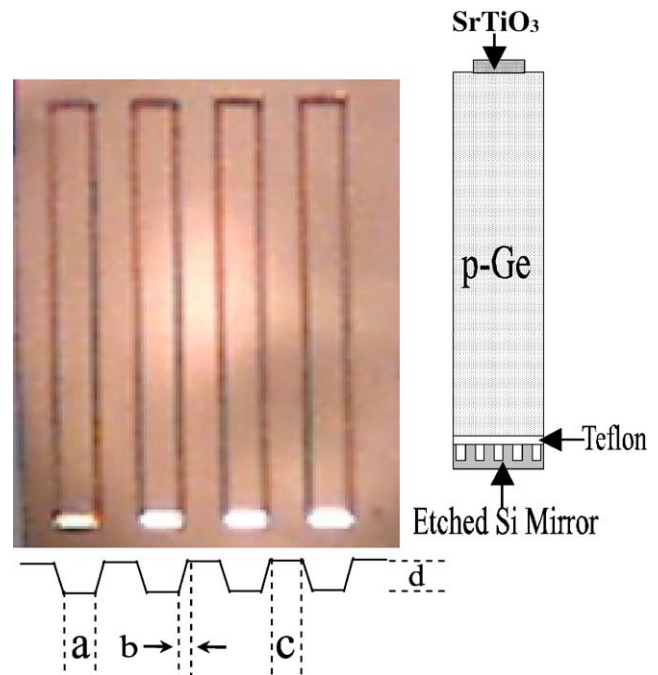


Fig. 1. (right) Schematic of the p-Ge laser with the silicon etched mirror used for wavelength selection. (left) Photograph of silicon etched mirror B after AuPd sputtering and Au evaporation. (bottom) Schematic definition of mirror geometrical parameters.

chipping the silicon with a scalpel. Roughness was determined at several locations in the trenches and on the top surface. The thickness of the metal coating was confirmed by measuring a pinhole that exposed the silicon surface.

The laser active crystals were made from the p-type germanium purchased from Tydex (St. Petersburg, Russia). The crystals were cut into rectangular rods of dimensions 45.75 mm \times 5.90 mm \times 2.65 mm (crystal 1) and 44.95 mm \times 5.80 mm \times 2.85 mm (crystal 2) with crystallographic orientations of its three axis as [1 1 0], [1 $\bar{1}$ 0] and [1 0 0], respectively. The length of the crystals defined a longitudinal mode separation of $\sim 0.028 \text{ cm}^{-1}$ for each, using an index of refraction of Ge at 4 K and 100 μm wavelength of 3.925 [13]. End faces were hand polished flat and parallel within 30 arcsec by a technique described in Ref. [14]. Indium ohmic contacts were applied to opposite [1 $\bar{1}$ 0] lateral faces with an ultrasonic soldering iron [14]. Electric field pulses with 1–2 μs duration were applied to an active crystal in the [1 $\bar{1}$ 0] direction with a thyatron pulser at repetition rates of 1–8 Hz. A magnetic field was applied along [1 1 0] active crystal axis using a home-built superconducting solenoid. The laser cavity construction, shown in Fig. 1, consists of the lamellar selective mirror, 20 μm Teflon film, the active crystal, and the SrTiO_3 output mirror, which is smaller than the active crystal end face to allow output coupling around its edges. The output laser radiation was detected by a 4 K Ge:Ga detector or a 4 K Si bolometer. Spectra of the output laser radiation were

collected on a Bomem DA8 vacuum-bench Fourier spectrometer using an Event-Locking [15] accessory (Zaubertek) at resolution of 0.5 cm^{-1} . Boxcar apodization gave an instrumental linewidth (FWHM) of 0.302 cm^{-1} [16]. A Mylar pellicle beam-splitter and a 4 K silicon composite bolometer (Infrared Labs) were used.

3. Results

Fig. 1 shows a photograph of mirror B. The schematic profile indicates the geometrical parameters collected in Table 1 for both mirrors A and B. Fig. 2 shows the AFM results for mirror B. The average roughness (R_a) of the trench surface is $10 \pm 2 \text{ nm}$ with an rms roughness (R_q) of $18 \pm 3 \text{ nm}$. The surface irregularities were uniform throughout the mirror. From a pinhole defect, a 650 nm thickness was measured for the applied metal (Au+AuPd), which is within 50 nm of the estimate made at the time of deposition. In the trenches of the mirror, the silicon etching created $\sim 100 \text{ nm}$ deep $\times 30 \text{ nm}$ wide scallops.

Fig. 3 shows the laser operation zone in the space of applied \mathbf{E} and \mathbf{B} fields using laser crystal 1 and mirror A. This zone is compared to that of the same laser with a SrTiO_3 back mirror instead of mirror A. The electric field threshold using the selector mirror is higher than that found when using the broadband mirror, which is an indication of larger radiative losses.

Fig. 4 presents p-Ge laser emission spectra using mirror A with laser crystal 1. This spectrum was obtained from a single scan of the interferometer mirror, i.e. without co-addition, and the interferogram was transformed at the lower resolution of 1 cm^{-1} to reduce the noise. Evidence of wavelength selection by the etched mirror is clear. A single line is observed at 103.3 cm^{-1} ($96.8 \mu\text{m}$ wavelength) and no other emission lines are observed throughout the $50\text{--}140 \text{ cm}^{-1}$ range of the p-Ge laser. The observed line width is that of the instrument at the chosen resolution. Hence, mirror A provides selectivity with at least $0.028/0.604 = 0.046$ active cavity finesse determined by the ratio of the longitudinal mode separation to the instrumental line width.

Table 1
Experimental and theoretical parameters associated with the lamellar selectors

Selector, crystal	A,1	B,2
a (μm)	150.4	414.0
b (μm)	95.3	94.9
c (μm)	463.3	406.4
d (μm)	134 ± 5	126 ± 5
Period $a + 2b + c$ (μm)	804.3	1010.2
Observed Line (cm^{-1})	103.3 ± 0.6	112.7 ± 0.3
Calculated $m = 3$ resonance (cm^{-1})	111.9 ± 4.1	119.0 ± 4.7
R_{max}	85%	88%
$\beta(\text{cm}^{-1})$	0.018	0.014

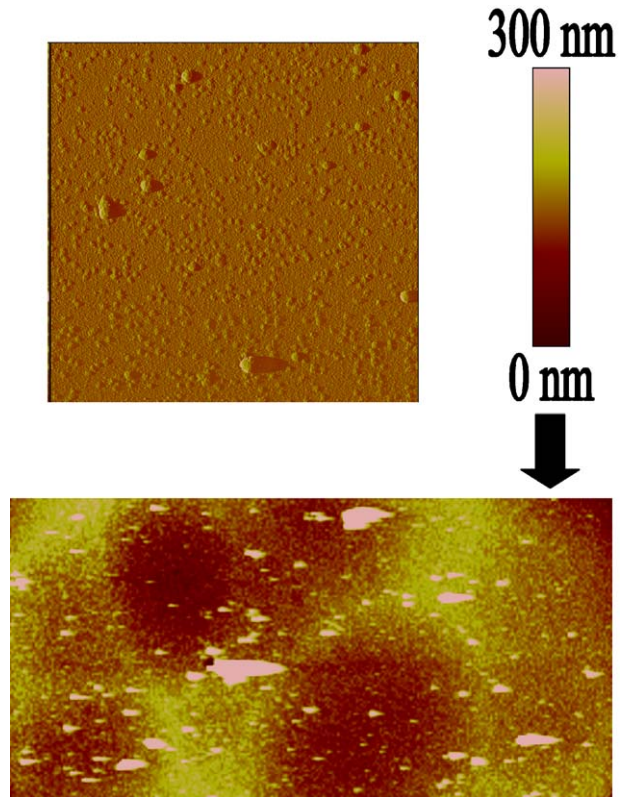


Fig. 2. (top) AFM error-signal mode results of a $10 \mu\text{m}$ square located in one of the trenches of the mirror. (bottom) An AFM height (topographical) image of a $110 \mu\text{m} \times 55 \mu\text{m}$ section of a trench showing scallops with diameter of $\sim 30 \mu\text{m}$ and depth $\sim 100 \text{ nm}$ created by the silicon etching. A second-order XY polynomial was subtracted to remove the scan curvature.

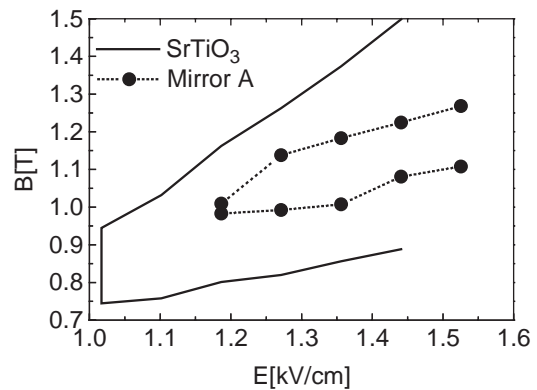


Fig. 3. Comparison of the laser generation zones using the wavelength-selecting mirror A or SrTiO_3 as back mirrors on laser crystal 1.

Results using mirror B with laser crystal 2 are also shown in Fig. 4. A single line is observed at 112.7 cm^{-1} ($88.7 \mu\text{m}$). The observed line width is that of the instrument at the chosen resolution. Hence, mirror B results in an active cavity finesse of at least $0.028/0.302 = 0.09$.

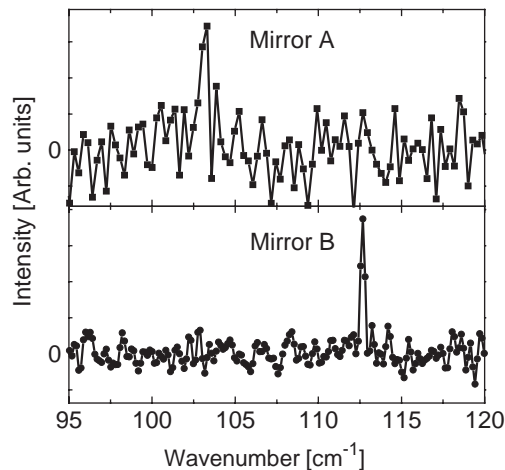


Fig. 4. Emission spectra of far-infrared p-Ge laser with the etched silicon wavelength selective mirror A (1 cm^{-1} resolution) and mirror B (0.5 cm^{-1} resolution).

4. Discussion

Normal lamellar grating reflections occur for resonances defined by

$$2d = m\lambda, \quad (1)$$

where d is the trench depth, λ is the wavelength of the laser light, and m is an integer. From the measured d values, both gratings appear to operate on the $m = 3$ resonance. Calculated and observed laser line positions are given in Table 1. The agreement is somewhat worse than the estimated uncertainty, which could be attributed to the $20 \text{ }\mu\text{m}$ Teflon film placed between the mirror and the laser crystal for electrical insulation.

Lamellar-patterned mirrors operating on resonance (Eq. (1)) should not introduce significant additional diffraction loss compared to plane mirrors. Assuming an effective beam diameter of the laser mode within the active crystal defined by the size of the output coupling mirror, approximately two periods of each lamellar mirror are illuminated. According to the far-field lamellar grating analysis given in Ref. [4], the FWHM angular divergence of the normal reflection peak is the same as one obtains from ordinary diffraction on reflection from a plane mirror of the same dimension.

Detuning out of the resonance causes step-like variations of the reflected phase front, which leads to re-emission of the incident radiation into diffraction lobes at the angles $\sin(\theta) = \lambda/(a + 2b + c)$. For the wavelength in vacuum $100 \text{ }\mu\text{m}$, $\theta = 1.8$ (31) and 1.4 (25) degrees (mrad) for A and B mirror, respectively (using $\lambda \sim 25 \text{ }\mu\text{m}$ inside Ge). Considering that the angular size of the output mirror is $40\text{--}50$ mrad, this radiation will leave the cavity after 2 roundtrips, causing remarkable loss for off-resonance radiation.

The higher threshold in Fig. 3 indicates that mirror A is lossy compared to usual metal or SrTiO_3 mirrors. This

can be explained by a reduction of the total gain caused by sloping sidewalls of the lamellar trenches. An upper bound for the lamellar mirror reflectivity R at resonance (Eq. (1)) can be estimated for incident plane waves as

$$R_{\max} \leq (a + c + R_{\text{Ge}} * 2b)/(a + c + 2b), \quad (2)$$

where R_{Ge} is reflection coefficient from the Ge/vacuum interface, $R_{\text{Ge}} = 35\%$, and (a, b, c) are the geometrical selector parameters (Fig. 1 and Table 1). Influence of the Teflon film between the mirror and the active crystal is ignored. R_{\max} values for the two mirrors are given in Table 1. Considering that gain α and mirror reflectivity R satisfy the condition

$$R \text{Exp}(2\alpha L_{\text{Ge}}) \geq 1, \quad (3)$$

the estimated effective minimum lamellar mirror loss (for plane waves), β , can be expressed as

$$\beta = \ln(1/R_{\max})/(2L_{\text{Ge}}), \quad (4)$$

where L_{Ge} is the length of the Ge laser cavity. Calculated β values (Table 1) are smaller than the most reported gain values, which are in the range $0.01\text{--}0.1 \text{ cm}^{-1}$ [1], consistent with the fact of laser operation using the lamellar mirrors. In reality, the mirror losses at resonance must be smaller than the Table 1 estimates, which assumed plane waves, because in an active laser cavity the mode profile will automatically optimize to achieve minimum loss.

Etching produces uniform trenches with roughness much less than the laser wavelength and hence is a suitable fabrication technique for far-IR selective laser mirrors. Less than ideal performance, as indicated by the higher threshold (Fig. 3), can be attributed mostly to loss on the sloping side walls, though particulates on the surface (Fig. 2) may contribute. No special care was paid to surface cleanliness during metal deposition so there is room for improvement. Higher threshold also may be attributed to problems with Teflon film. This interpretation is supported by the observation that the laser failed to operate after a thermal cycling unless the Teflon film was changed. A possible solution would be to spin on a polymer after gold coating to electrically insulate the mirror from the high-voltage contacts.

5. Conclusions

A robust and simple device based on patterned silicon was demonstrated for predetermined fixed wavelength intracavity selection in the broadly tunable far-infrared p-Ge laser. The best laser line width was less than 0.3 cm^{-1} giving an active cavity finesse of at least 0.09. A p-Ge laser equipped with such a selector easily can be prepared to operate in regions of relatively high atmospheric transmission for applications in chemical sensing, THz imaging, and non-destructive testing. The same processing technique can be used to create more complicated selective mirrors, for example with multiple depths.

Acknowledgements

This work was partially supported by NSF Grant ECS-0070228 to UCF and AFOSR F49620-02-C-0027 SBIR Phase II to Zaubertek.

References

- [1] Bründermann E. Widely tunable far-infrared hot-hole semiconductor lasers. In: Choi HK, editor. Long-wavelength infrared semiconductor lasers. Hoboken, New Jersey: Wiley-Interscience; 2004. p 279–350.
- [2] Williams BS, Callebaut H, Kumar S, Hu Q, Reno JL. 3.4 THz quantum cascade laser based on longitudinal-optical-phonon scattering for depopulation. *Appl Phys Lett* 2003;82(7):1015–7.
- [3] Köhler R, Tredicucci A, Beltram F, Beere HE, Linfield EH, Davies AG, Ritchie DA, Iotti RC, Rossi F. Terahertz semiconductor–heterostructure laser. *Nature* 2002;417(6885):156–9.
- [4] Strong J, Vanasse GA. Lamellar grating far-infrared interferometer. *J Opt Soc Am* 1960;50(2):113–8.
- [5] Murav'ev AV, Nefedov IM, Pavlov SG, Shastin VN. Tunable narrowband laser that operates on interband transitions of hot holes in germanium. *Quantum Electron* 1993;23(2):119–24.
- [6] Komiyama S, Morita H, Hosako I. Continuous wavelength tuning of inter-valence-band laser oscillation in p-type germanium over range of 80–120 μm . *Jpn J Appl Phys* 1993;32(11A):4987–91.
- [7] Muravjov AV, Withers SH, Weidner H, Strijbos RC, Pavlov SG, Shastin VN, Peale RE. Single axial-mode selection in a far-infrared p-Ge laser. *Appl Phys Lett* 2000;76(15):1996–8.
- [8] Nelson EW, Muravjov AV, Pavlov SG, Shastin VN, Peale RE. Piezo controlled intracavity wavelength selector for the far-infrared p-Ge laser. *Infrared Phys Technol* 2001;42:107–10.
- [9] Muravjov AV, Nelson EW, Peale RE, Shastin VN, Fredricksen CJ. Far-infrared p-Ge laser with variable length cavity. *Infrared Phys Technol* 2003;44:75–8.
- [10] Nelson EW, Withers SH, Muravjov AV, Strijbos RC, Peale RE, Pavlov SG, Shastin VN, Fredricksen CJ. High-resolution study of composite cavity effects for p-Ge lasers. *IEEE J Quantum Electron* 2001;37(12):1525–30.
- [11] Du Bosq TW, Peale RE, Nelson EW, Muravjov AV, Fredricksen CJ. Fixed wavelength selection for the far-infrared p-Ge laser using thin silicon intracavity etalon. In: Scheps R, editor. *Solid State Lasers XII*. Proc SPIE 2003;4968:18–23.
- [12] Du Bosq TW, Peale RE, Nelson EW, Muravjov AV, Fredricksen CJ, Tache N, Tanner DB. Dielectric selective mirror for intracavity wavelength selection in far-infrared p-Ge lasers. *J Appl Phys* 2003; 94(9):5474–8.
- [13] Loewenstein EV, Smith DR, Morgan RL. Optical constants of far infrared materials 2: crystalline solids. *Appl Opt* 1973;12(2): 398–406.
- [14] Nelson EW. Neutron transmutation doped p-Ge laser. Ph.D. dissertation. Orlando: University of Central Florida; 2003.
- [15] Weidner H, Peale RE. Event-locked time-resolved Fourier Spectroscopy. *Appl Spectrosc* 1997;51(8):1106–12.
- [16] Bell RG. *Introductory fourier transform spectroscopy*. Burlington MA:Academic Press; 1972.